Journal of
Composites Science

MDPI

Article

Strain Control of Magnetic Anisotropy in Yttrium Iron Garnet Films in a Composite Structure with Yttrium Aluminum Garnet Substrate

Ying Liu [1,2], Peng Zhou [2], Rao Bidthanapally [1], Jitao Zhang [3], Wei Zhang [1], Michael R. Page [4], Tianjin Zhang [2] and Gopalan Srinivasan [1,*]

[1] Department of Physics, Oakland University, Rochester, MI 48309, USA; liuying.hube@outlook.com (Y.L.); burao@oakland.edu (R.B.); weizhang@oakalnd.edu (W.Z.)
[2] Department of Materials Science and Engineering, Hubei University, Wuhan 430062, China; p_zhou@outlook.com (P.Z.); zhangtj@hubu.edu.cn (T.Z.)
[3] College of Electrical and Information Engineering, Zhengzhou University of Light Industry, Zhengzhou 450002, China; zhang_jitao@outlook.com
[4] Materials and Manufacturing Directorate, Air Force Research Laboratory, Wright-Patterson Air Force Base, Dayton, OH 45433, USA; michael.page.16@us.af.mil
* Correspondence: srinivas@oakland.edu

Abstract: This report is on the nature of strain in thin films of yttrium iron garnet (YIG) on yttrium aluminum garnet (YAG) substrates due to film-substrate lattice mismatch and the resulting induced magnetic anisotropy. Films with thickness 55 nm to 380 nm were deposited on (100), (110), and (111) YAG substrates using pulsed laser deposition (PLD) techniques and characterized by structural and magnetic characterization techniques. The in-plane strain determined to be compressive using X-ray diffraction (XRD). It varied from −0.12% to −0.98% and increased in magnitude with increasing film thickness and was relatively large in films on (100) YAG. The out-of-plane strain was tensile and also increased with increasing film thickness. The estimated strain-induced magnetic anisotropy field, found from XRD data, was out of plane; its value increased with film thickness and ranged from 0.47 kOe to 3.96 kOe. Ferromagnetic resonance (FMR) measurements at 5 to 21 GHz also revealed the presence of a perpendicular magnetic anisotropy that decreased with increasing film thickness and its values were smaller than values obtained from XRD data. The PLD YIG films on YAG substrates exhibiting a perpendicular anisotropy field have the potential for use in self-biased sensors and high-frequency devices.

Keywords: yttrium iron garnet; yttrium aluminum garnet; ferrimagnets; thin films; strain anisotropy field; growth-induced magnetic anisotropy

Citation: Liu, Y.; Zhou, P.; Bidthanapally, R.; Zhang, J.; Zhang, W.; Page, M.R.; Zhang, T.; Srinivasan, G. Strain Control of Magnetic Anisotropy in Yttrium Iron Garnet Films in a Composite Structure with Yttrium Aluminum Garnet Substrate. *J. Compos. Sci.* **2022**, *6*, 203. https://doi.org/10.3390/jcs6070203

Academic Editors: Francesco Tornabene and Konda Gokuldoss Prashanth

Received: 3 May 2022
Accepted: 6 July 2022
Published: 12 July 2022

1. Introduction

Yttrium iron garnet (YIG) and rare-earth iron garnets (RIGs) are ferrimagnetic oxides with a Curie temperature well above room temperature [1–3]. Bismuth-substituted YIG and several RIGs show high Faraday rotation and are useful for applications such as magnetic field sensors [4–6]. YIG is one of the materials with the lowest losses at high frequencies and is used in microwave devices including resonators, filters, and RF sensors [7–11]. Spin waves in nano-structures of YIG, referred to as YIG magnonics, are of interest for information storage and processing technologies [7]. Related recent developments in the application aspects of ferrimagnetic garnets are the demonstration of YIG-ferroelectric composites for magnetic field sensors and voltage tunable high-frequency devices [12–15]. YIG is also of interest for use in devices based on spin torque transfer phenomena [16,17]. In most of these applications, the need for a bias magnetic field renders their miniaturization hard to realize. For example, in the case of devices utilizing hexagonal ferrites with a large uniaxial or planar magnetocrystalline anisotropy field, it might be possible to eliminate the

need for a bias magnetic field, but YIG has a low magnetocrystalline anisotropy field on the order of 50 Oe [18].

There were several attempts in the past to enhance the anisotropy field H_a in ferromagnetic thin films and nanocrystalline crystalline materials [19,20]. In the case of thin ferrimagnetic films, it is possible to achieve a significant enhancement in H_a by substitutions, controlling the oxygen stoichiometry, or by film-substrate lattice mismatch [21–27]. For example, in ultrathin pure and Zn-substituted nickel ferrite films on magnesium aluminate and some gallate substrates H_a to the order 10 to 15 kOe were previously reported [26,27]. Thin films of YIG on yttrium aluminum garnet (YAG) has attracted considerable interest for achieving a large perpendicular magnetic anisotropy [28–34]. The lattice constants of YIG and YAG are 12.376 Å and 12.009 Å, respectively, and the −3% mismatch is expected to result in a compressive in-plane strain and a tensile strain perpendicular to the film plane [35]. A recent report predicted a strain-induced uniaxial H_a on the order of 2.6 kOe for YIG films on YAG substrates [35].

Past efforts on deposition of YIG films utilized a variety of deposition techniques including chemical vapor deposition (CVD), RF sputtering, and pulsed laser deposition (PLD) [28–34,36]. In techniques such as RF sputtering and CVD, film stoichiometry is critically dependent on parameters such as chamber pressure and substrate temperatures. PLD, however, has several advantages including preservation of target stoichiometry in the film [37]. In addition, films could be deposited under a wide range of chamber pressure and substrate temperatures since the laser source is external to the deposition chamber [37].

Early works on deposition of YIG films on YAG involved CVD techniques and reported an in-plane tensile strain primarily due to the thermal expansion mismatch between the film and the substrate [29]. Rapid deposition of YIG on YAG by the metallo-organic CVD technique was found to result in YIG films with a high magnetization due to the presence of divalent Fe [30]. A recent report on PLD deposition of amorphous YIG on (100) YAG and subsequent recrystallization also resulted in an in-plane tensile strain [32]. Wang et al. reported an out-of-plane uniaxial H_a that decreased from 1252 Oe in 9.8 nm-thick YIG films on (100) YAG to 49 Oe in 72.7 nm-thick films prepared by sputtering techniques [34]. One, however, prefers YIG films with a thickness of at least 0.5 to 1 μm for applications for sensors and microwave devices.

We report here the deposition by PLD techniques on YIG films of thickness 55 nm to 380 nm on (100), (110), and (111) YAG substrates, and the results of a systematic study on the structural and magnetic properties. The films deposited at 650 °C and annealed at 1000 °C showed an increase in the out-of-plane lattice constant c and a decrease in the in-plane lattice constant a with increasing film thickness. The estimated strain anisotropy H_δ from X-ray diffraction data was uniaxial and perpendicular to the film plane, and increased with increasing film thickness. The room temperature magnetization, $4\pi M_s$, is in the range 1700–2000 G, which was in general agreement with values for bulk single crystal YIG. Ferromagnetic resonance (FMR) measurements at 5–21 GHz indicated a uniaxial anisotropy of 20 Oe to 450 Oe that generally decreases with increasing film thickness with the maximum values for films on (111) YAG. The FMR line-width ΔH ranged from 19.5 Oe to 92 Oe for the films on (100). YAG showed the lowest ΔH. Details on our study are presented in the sections that follow.

2. Experimental Section

The target of yttrium iron garnet for the deposition of films was synthesized using traditional ceramic processing techniques from yttrium oxide (Y_2O_3) and iron oxide (Fe_2O_3). First, the oxides (11.475 g Y_2O_3 and 13.525 g Fe_2O_3) were mixed with 12.5 mL methanol in the ratio of 2:1 in a ball mill for 12 h and dried for 12 h at room temperature. Then, the powder was pre-sintered at 950 °C for 6 h with a heating rate of 2 °C/min. The sintered powders were ground to fine particles and ball-milled for 24 h. Finally, the mixture was dried at room temperature and pressed into a disk with diameter of 6 cm and thickness of 3 cm, then sintered at 1525 °C for 15 h with the heating rate of 2 °C/min. The disk of

YIG was used as a target in the PLD system. Films of YIG were deposited for a duration of 30–120 min on (100), (110), and (111) and oriented on 0.5 mm-thick YAG substrates. The growth temperature for all the films was 650 °C at an oxygen pressure of 1.0 Pa. The distance between target and substrates was 5 cm and the laser pulse energy was 300 mJ (krypton fluoride, KrF) at a frequency of 5 Hz. Following the deposition, the samples were cooled at a rate of 2 °C/min. All samples were post annealed at 1000 °C in an oxygen atmosphere for 2 h with a heating and cooling rate of 2 °C/min.

Film thickness was measured using cross-section scanning electron microscopy (SEM) images, while film composition was determined using energy dispersive X-ray spectroscopy. There have been several reports that describe measurements of strain anisotropy in magnetic materials. Techniques employed include θ–2θ patterns in X-ray diffraction (XRD), XRD pole figures, XRD phi-scan, XRD reciprocal space mapping, transmission electron microscopy, ferromagnetic resonance, and magnetization vs. static field [19,20,25–27]. In this work, XRD and FMR data were utilized for the calculations of strain as well as strain-induced magnetic anisotropy field. XRD patterns for the YIG target and films were obtained at room temperature using a powder diffraction system Bruker XRD, D8 Advance, Cu K_α, λ = 1.5406 Å, (Bruker Instruments, Billerica, MA, USA). Imaging of the magnetic domains for YIG films was carried out using a magnetic force microscope (MFM) with a Basic Atomic Force Microscope (B-AFM) (AFM Workshop, Hilton Head, SC, USA). The magnetization measurement was conducted at room temperature using a Faraday balance. Ferromagnetic resonance (FMR) measurements were performed with the films placed in a coplanar waveguide that was excited with microwave power using a Vector Network Analyzer (VNA) (Agilent Technologies, Denver, CO, USA). The DC bias magnetic field was applied parallel to the sample plane. Profiles of FMR were recorded by measuring the amplitude of the scattering matrix parameter S_{12} vs. frequency f as a function of bias magnetic field H values and also by recoding the derivative of the power absorbed dP/dH as a function of f for a series of frequencies from 5 to 21 GHz.

3. Results

YIG films were deposited for durations of 30, 60, 90, and 120 min. Figure 1 shows cross sectional SEM images for films deposited on (100) YAG. The deposition rate varied from 1.83 nm/min to 3.17 nm/min for film thicknesses of 55–380 nm. Figures S1–S8 in the supplement show similar SEM images used for thickness measurements for films on (110) and (111) YAG. Table 1 shows the YIG film thickness as a function of deposition time for all orientations of YAG substrate. Surface topography of the films were probed with an AFM.

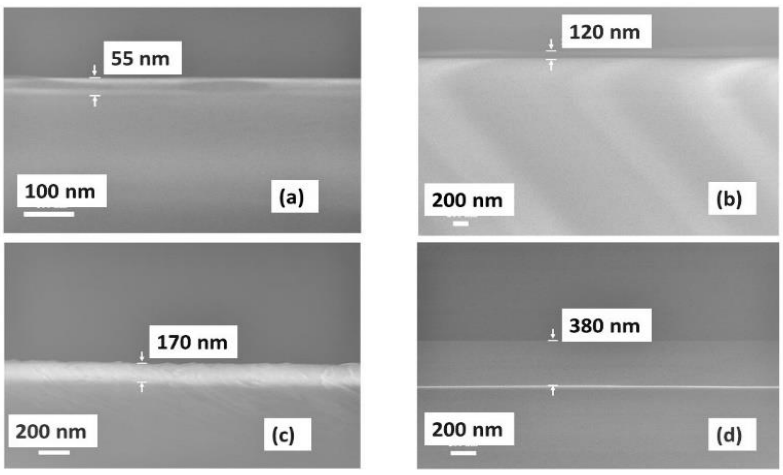

Figure 1. SEM cross-sectional images showing the thickness of YIG films deposited for (**a**) 30, (**b**) 60, (**c**) 90, and (**d**) 120 min on (100) YAG.

Table 1. Thickness of YIG films on (100), (110), and (111) YAG as a function of deposition time. Estimated out-of-plane lattice constant c, in-plane lattice constant a, the out of plane strain ε_{zz}, and in-plane strain ε_{xx} for YIG films on YAG (100), (110), and (111) substrates.

Film	Deposition Time	Thickness (±5%)	c (Å)	a (Å)	ε_{zz}	ε_{xx}
YIG/YAG (100)	30 min	55 nm	12.440	12.344	0.52%	−0.26%
	60 min	120 nm	12.492	12.318	0.94%	−0.47%
	90 min	170 nm	12.544	12.293	1.36%	−0.67%
	120 min	380 nm	12.624	12.254	2.00%	−0.98%
YIG/YAG (110)	30 min	91 nm	12.405	12.361	0.23%	−0.12%
	60 min	145 nm	12.462	12.333	0.69%	−0.35%
	90 min	171 nm	12.484	12.322	0.87%	−0.44%
	120 min	205 nm	12.524	12.303	1.19%	−0.59%
YIG/YAG (111)	30 min	127 nm	12.429	12.355	0.43%	−0.17%
	60 min	171 nm	12.464	12.338	0.71%	−0.31%
	90 min	274 nm	12.491	12.325	0.93%	−0.41%
	120 min	357 nm	12.533	12.304	1.27%	−0.58%

Figure 2 shows representative AFM images for films on (100) YAG. The images show smooth surface with a roughness of around 2 nm. Chemical composition for the films was determined using energy dispersive X-ray spectroscopy and was found to be $Y_{3\pm0.02}$ $Fe_{5\pm0.05}$ O_{12}, which was close to the stoichiometric composition (Figure S9 in the supplementary file shows representative composition data).

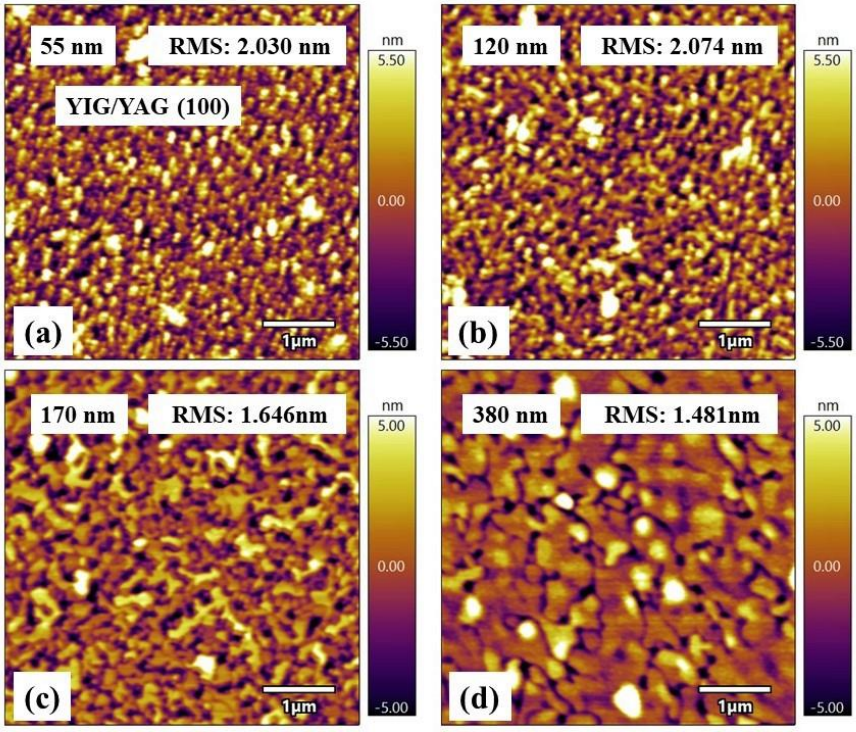

Figure 2. AFM topography images for YIG films of thickness (**a**) 55 nm, (**b**) 120 nm, (**c**) 170 nm, and (**d**) 380 nm on (100) YAG.

The film crystal structure was studied via X-ray diffraction. Figure 3 shows the XRD θ–2θ plots for the YIG films on YAG substrates for (100), (110), and (111) orientations. All the YIG films were grown on YAG substrates showing the (400), (440), or (444) diffraction peaks. The (400) diffraction peaks in Figure 3a shift to the right toward the YAG peaks when the thickness of the films is decreased. A similar shift closer to the YAG peaks with

decreasing film thickness is also observed for (440) and (444) peaks for the films on (110) and (111) YAG substrates, respectively. The out-of-plane lattice constants c for the YIG films obtained from the XRD scans using the Bragg formulation are listed in Table 1, which shows an increase when the film thickness increased. The lattice constant for bulk YIG a_b was found to be 12.376 Å [34,38,39]. The in-plane lattice constant a for the films can be estimated from the unit cell volume for bulk YIG and c-values in Table 1, and is given by $a = (12.376)^{3/2}/c$ Å. Values of a as a function of the film thickness are also listed in Table 1.

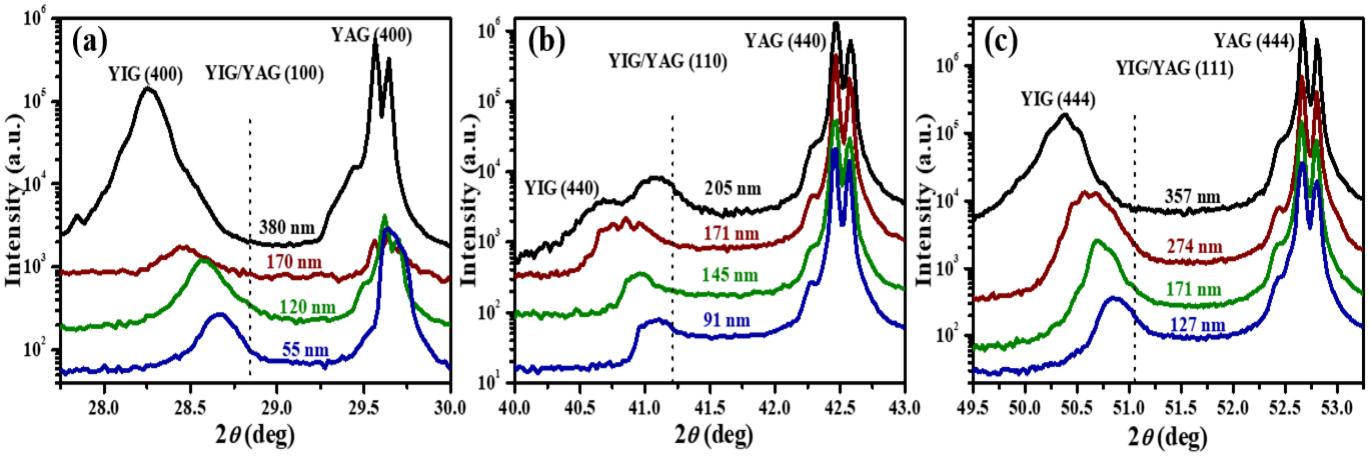

Figure 3. (**a**) XRD patterns for the YIG film on (**a**) (100), (**b**) (110), and (**c**) (111) YAG substrates. The positions of the dotted lines in the figure represent the diffraction peaks of the corresponding orientation of bulk YIG.

The out-of-plane strain ε_{zz} for the YIG films was calculated using the expression $\varepsilon_{zz} = \frac{c - a_b}{a_b}$, where a_b is the lattice constant for bulk YIG. The in-plane strain ε_{xx} can be estimated from $\varepsilon_{xx} = (a - a_b)/a_b$. Values of the estimated in-plane and out-of-plane strains are listed in Table 1 and, as expected, the strains were compressive and tensile, respectively. First, we will consider the lattice constants and strain values in Table 1 for the films on (111) YAG. The a-value for the 127 nm-thick film was close to that of bulk YIG values, which decreased when film thickness increased. This was accompanied by an increase in the magnitude of compressive ε_{xx} from 0.17% for the 127 nm-thick film to 0.58% for the 357 nm film. Values of c and the tensile strain ε_{zz} both increased when film thickness increased. These observations are contrary to the expectations that the a value for the thinnest film should be close to the YAG substrate, and that both strains should relax and decrease in their magnitudes when film thickness increases. The films on (110) and (111) also showed a similar dependence of lattice constants and strains on YIG film thickness. Further, the films on (100) YAG substrate showed the maximum values for both in-plane and out-of-plane strains.

The variations in the lattice constants and strains with the film thickness in our system was similar to the findings reported in [32] for films of YIG on (100) YAG. In that study, amorphous films of YIG were deposited on unheated YAG substrates and then annealed at 800 °C to obtain crystalline films. As in the present study, a similar decrease in the in-plane lattice constant a and an increase in the c-value were reported as the film thickness increased from 9.6 nm to 56 nm [32]. The authors attributed these observations to two causes: (i) tilting (rotation) of unit cell of YIG relative to YAG during the film growth and dislocations at the film-substrate interface; and (ii) the difference in the linear thermal expansion coefficient α for the film and the substrate that results in a tensile strain at the interface. YIG ($\alpha = 10 \times 10^{-6}/°C$) is a factor 4 greater than that of YAG ($\alpha = 2.7 \times 10^{-6}/°C$) [40,41]. In another study, the measured in-plane tensile strain in a 4 µm-thick YIG film on 1 mm-thick YAG substrate grown via CVD techniques at 1250 °C was accounted for by the mismatch in α [32]. In the present study (films grown at 650 °C and annealed at 1000 °C), instead of the anticipated $\varepsilon_{xx} \sim -3\%$, the observed $\varepsilon_{xx} = -0.26$ %

for the 55 nm film on (100) YAG and subsequent increase in its magnitude to −0.98% for the thickest film could be due to a combination of YIG–YAG compressive strain, which was caused by a lattice mismatch and a tensile strain due to difference in α-values. Films on other orientations of YAG substrates also showed a similar variation in the strains with film thickness. Estimates of the strain-induced anisotropy field H_σ are provided in the Discussion section.

The magnetic domain patterns for the thickest YIG films on (100), (110), and (111) YAG substrates were imaged by magnetic force microscope (MFM), as shown in Figure 4. A stripe domain pattern was observed for the YIG films. Our MFM measurement was performed by scanning a ferromagnetic probe over the film, which detected a perpendicular magnetic field gradient from the sample. The stripe domain-like structure of YIG films could be due to the pre-magnetization of the samples and the external magnetic field-induced alignment of the domain structure [42–46]. It is very likely that this out-of-plane magnetization is associated with the boundary between two neighboring domains with in-plane magnetization. The images, therefore, indicate that an out-of-plane component of the magnetization was present in the films.

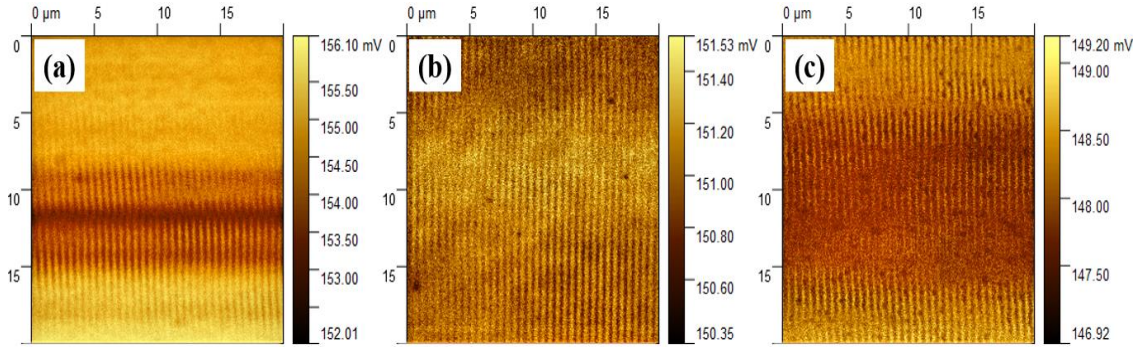

Figure 4. (**a**–**c**) MFM phase images showing the stripe domains in the thickest YIG films on (100), (110), and (111) YAG substrates.

The magnetization measurements at room temperature for the YIG films were performed with a Faraday balance. Figure 5 displays M vs. H hysteresis loops for the thickest YIG films for in-plane and out-of-plane H. The in-plane coercive field was less than 25 Oe and was the highest for the (110) YIG film and the lowest for the (100) YIG film. The saturation field H_s for in-plane loops was on the order of 200 Oe, whereas the out-of-plane H_s was in the range 1700–1800 Oe. The saturation induction $4\pi M_s$ for the films are listed in Table 2 and were found to be in the range 1700–1980 G, which was close to the value of 1750 G for bulk YIG [47]. Additional hysteresis loops for H in-plane and perpendicular to the film plane are shown in the supplement (Figures S10–S14). The magnetization values were used for the determination of the growth-induced anisotropy field from FMR measurements that are discussed next.

Ferromagnetic resonance measurements were carried out to determine the magnetic parameters for the films. For ferromagnetic resonance (FMR) measurements, we used a vector network analyzer [48–50]. Two types of measurements were done. (i) The VNA was used as a source of microwave power, and the sample placed in an S-shaped coplanar waveguide and subjected to a modulation field at 1 kHz were generated by a pair of Helmholtz coils and a static field H was generated by an electromagnet. Profiles derivative of the power dP/dH was recorded as a function of H with the use of lock-in detection [48]. This procedure was mainly used for determining FMR line width. (ii) Profiles of the amplitude of scattering matrix parameter S_{21} was recorded as a function of frequency f = 5–21 GHz with H applied either parallel or perpendicular to the sample plane. The FMR resonance frequency f_r was measured from the position of maximum absorption by the sample. The VNA was calibrated with the use of electronic calibration for these measurements. FMR measurements were done on all 12 YIG films. Figure 6 shows

representative profiles of dP/dH vs. H for the 357 nm-thick YIG/(111) YAG for in-plane H and f = 5–21 GHz. The resonance frequency f_r and the field H_r for in-plane applied fields are related by the Kittel equation:

$$f_r^2 = \gamma^2 (H_r + H_c)(H_r + H_c + 4\pi M_{eff}) \quad (1)$$

where γ is the gyromagnetic ratio, H_c is the magnetocrystalline anisotropy field, and the effective magnetization $4\pi M_{eff}$ is defined as $4\pi M_{eff} = 4\pi M_s + H_a$. Here, H_a is the strain induced magnetic anisotropy field, and it is assumed to be positive for in-plane field and negative for out-of-plane field. Our FMR measurements as a function of orientation of in-plane H did not show any measurable change in the resonance frequency or field and is indicative of a rather small magnetocrystalline anisotropy field H_c. A recent study on YIG films on YAG reported H_c on the order of 10–60 Oe [32]. We, therefore, did not take into consideration H_c in Equation (1). Data on the resonance frequency and field were fitted to Equation (1), as shown in Figure 6, to obtain the parameters γ = 2.79 GHz/kOe and $4\pi M_{eff}$ = 1.579 kG.

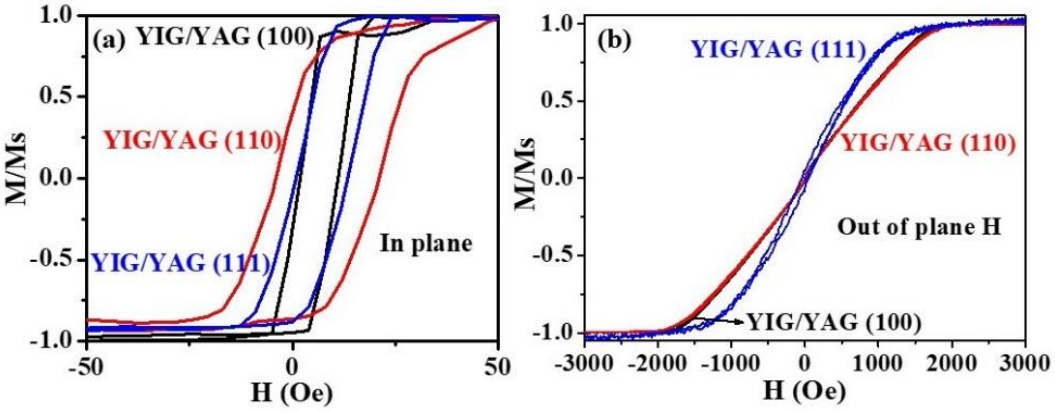

Figure 5. Normalized in plane (**a**) and out-of-plane (**b**) M-H hysteresis loops for the thickest YIG films grown on (100), (110), and (111) YAG substrates.

Table 2. The saturation induction $4\pi M_s$, gyromagtic ratio, and the effective saturation induction $4\pi M_{eff}$ for YIG films on YAG substrates.

Film	Thickness (nm)	$4\pi M_s$ (kG)	γ (GHz/kOe)	$4\pi M_{eff}$ (kG)
YIG/YAG (100)	55	1.80	2.80	1.35
	120	1.70	2.79	1.55
	170	1.80	2.77	1.64
	380	1.67	2.76	1.70
YIG/YAG (110)	91	1.70	2.77	1.44
	145	1.74	2.79	1.49
	171	1.80	2.78	1.60
	205	1.67	2.77	1.77
YIG/YAG (111)	127	1.71	2.79	1.36
	171	1.77	2.79	1.51
	274	1.98	2.78	1.53
	357	1.86	2.70	1.58

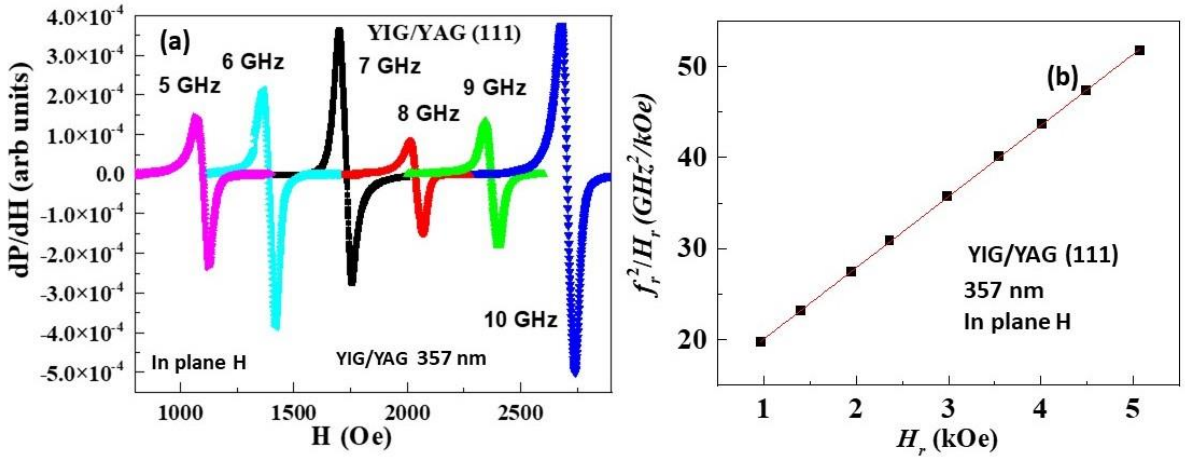

Figure 6. (**a**) Profiles of *dP/dH* vs. *H* showing FMR in 357 nm-thick YIG/(111) YAG for *H* applied parallel to film plane. (**b**) Theoretical fit to data on resonance frequency f_r and field H_r for estimation of magnetic parameters for the film.

FMR profiles of S_{21} vs. H for excitation frequencies from 14 to 21 GHz are shown in Figure 7 for 55 nm YIG film on (100) YAG. The in-plane field H was applied parallel to (001) of the film. The resonance appears as a sharp decrease in S_{21} and the figure also shows the fit to the data on resonance field and frequency. Estimated values of the magnetic parameters are γ = 2.8 GHz/kOe and $4\pi M_{eff}$ = 1.35 kG. The values of γ determined from the FMR data in Figures 6 and 7 agree with the value of 2.8 GHz/kOe for single crystal YIG [47]. Similar FMR measurements were also done on YIG/(110) YAG films with H applied parallel to (001). The parameters γ and $4\pi M_{eff}$ for all of the films obtained from data as in Figures 6 and 7 are listed in Table 2. Additional S_{21} vs. f profiles as in Figure 7 for FMR are shown in the Supplement (Figures S15–S19).

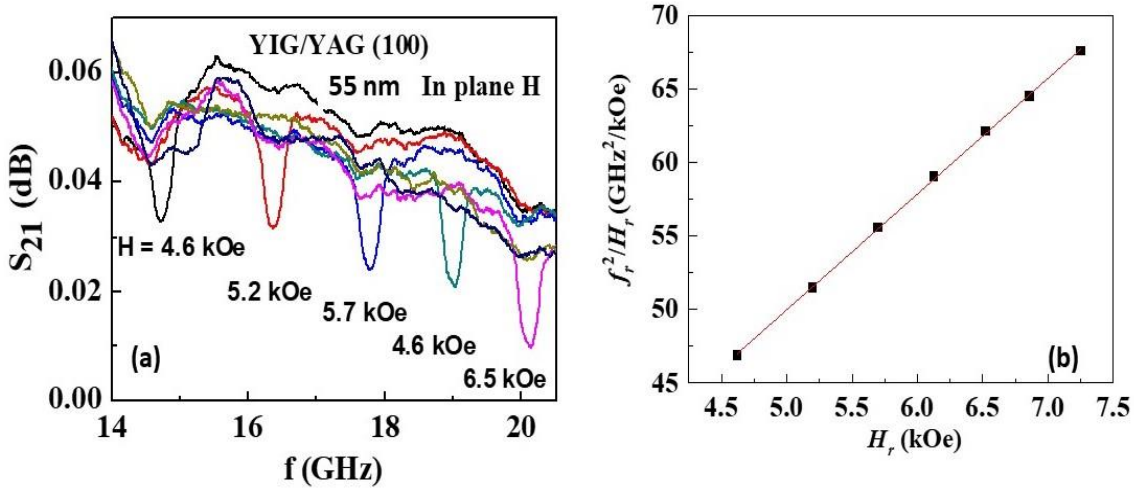

Figure 7. (**a**) Profiles of amplitude scattering matrix S_{21} vs. H showing FMR in 55 nm thick YIG/(100) YAG for in-plane H along (001) direction of YAG. (**b**) Theoretical fit to data on resonance frequency and field for estimation of magnetic parameters for the film.

The FMR line-width ΔH for the films was determined from profiles, such as in Figure 6. Figure 8 shows the measured peak-to-peak ΔH values for the thickest YIG films on YAG substrates for excitation frequencies from 5 to 10 GHz. The line width increased when frequencies increased for films of all three orientations on YAG. Films on (100) YAG showed the smallest ΔH value, which increased from 19.2 Oe at 5 GHz to 22 Oe at 10 GHz. Films on (111) YAG have ΔH = 50 Oe to 60 Oe for the same frequency range. Films on (110) YAG

showed the highest values for line-width, with ΔH increasing from 70 Oe at 5 GHz to 90 Oe at 10 GHz. The line-widths in Figure 8 for the films generally agree with ΔH reported for films on YIG on (100) YAG [32,34]. The linewidth of 205 nm YIG film on (110) YAG was higher than that of the films on (100) and (111) YAG, and the relatively large DH for the film compared to values in the literature for bulk single crystal YIG [47] could be due to the poor crystallinity of the sample. According to the XRD data in Figure 3, the Bragg peak of 205 nm YIG film was broadened and split into two peaks, showing a twinning-like behavior, and may be the cause of a large FMR linewidth. The determination of the growth induced magnetic anisotropy field for the films is considered in the following section.

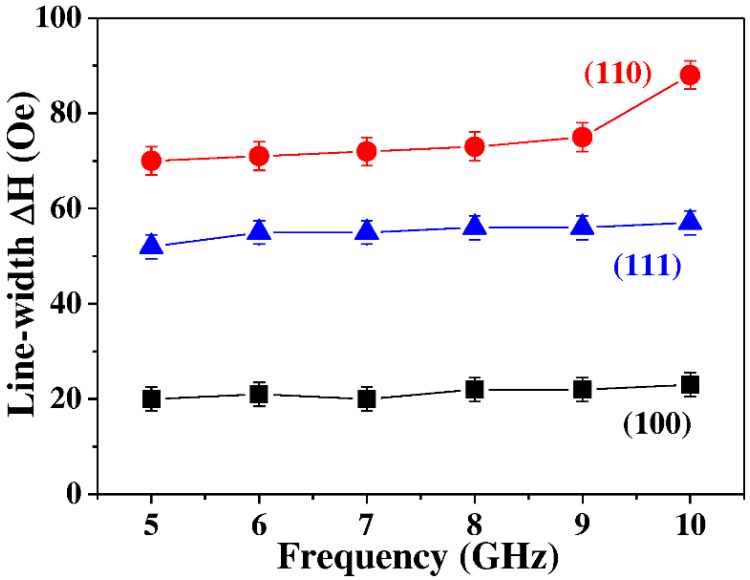

Figure 8. Dependence of FMR line-width ΔH on film thickness for 380 nm thick YIG film grown on (100) YAG, 205 nm film on (110) YAG, and 357 nm film on (111) YAG substrates. The ± 3 Oe error bars of FMR line-width are presented in the figure.

4. Discussion

In this section, we will discuss the results of this comprehensive study on the structural and magnetic properties of YIG films on the three different orientations of YAG substrates. Films with thicknesses of 55–380 nm were deposited by PLD techniques and, following the growth, annealed at 1000 °C in oxygen atmosphere. X-ray diffraction data confirmed the absence of any impurity phases and epitaxial nature of the films. Significant findings from the XRD measurements are as follows. (i) For all three substrate orientations, the thinnest films had in-plane lattice constants a close to that of YIG rather than the anticipated a value for YAG. (ii) With increasing film thickness, a-value decreased and the out-of-plane lattice constant c increased. (iii) The in-plane strain was compressive, the out-of-plane strain tensile, and the magnitude of both strains increased when film thickness increased. (iv) Although the -3% lattice match for YIG films on YAG was expected to be the determining factor in the growth of ultrathin films [30], the thermal expansion between YIG and YAG seemed to be the key factor that determined the structure and growth-induced strains for films annealed at high temperatures, as was the case for our films. This observation agrees with similar findings in previous reports on YIG films on YAG [29,32].

Next, we estimated the strain induced anisotropy field H_σ from the lattice constants, as shown in Table 1. The field H_σ is given by [26]

$$H_\sigma = 3\,\lambda\,\sigma/M_s, \quad (2)$$

where λ is the magnetostriction and σ is the effective strain given by

$$\sigma = (a - c)\ 2\ E/[a_b\ (1 + \nu)] \quad (3)$$

In Equation (3), a, c, and a_b are the in-plane and out-of-plane lattice constants for the YIG film and the lattice constant for bulk YIG, respectively, E is the Young's modulus and ν is the poison's ratio. Using Equations (2) and (3), as well as values a and c in Table 1, a_b = 1.2376 nm, $E = 2 \times 10^{12}$ dynes/cm^2, $\lambda = -2$ ppm, ν = 0.295, and M_s = 140 emu/cc, calculated H_σ values are listed in Table 3. Positive values of H_σ indicate easy plane anisotropy field, whereas negative values of H_σ are for uniaxial anisotropy field perpendicular to film plane. The anisotropy fields H_σ in Table 3 are uniaxial and showed to increase with increasing film thickness for all YAG substrate orientations. Films on (100) YAG were shown to have the highest H_σ value; its magnitude increased from 1 kOe for 55 nm film to 4 kOe for the thickest film. Films on (110) and (111) YAG substrates had H_σ of approximately the same value. The thickest films on (100), (110), and (111) YAG had H_σ= 2.4–4.0 kOe, which was in agreement with recent theoretical predictions [35].

Table 3. The strain anisotropy field H_σ estimated from XRD data and growth induced anisotropy field H_a determined from FMR data.

Film	Thickness (nm)	H_σ (kOe)	H_a (kOe)
YIG/YAG (100)	55	−1.02	−0.45
	120	−1.86	−0.15
	170	−2.69	−0.16
	380	−3.96	−0.03
YIG/YAG (110)	91	−0.47	−0.26
	145	−1.38	−0.25
	171	−1.73	−0.20
	205	−2.36	0
YIG/YAG (111)	127	−0.79	−0.35
	171	−1.35	−0.26
	274	−1.78	−0.44
	357	−2.45	−0.28

The MFM images in Figure 4 for the domain structure in the magnetized YIG films show stripe domains due to an out-of-plane component for the magnetization. The saturation magnetization $4\pi M_s$ measured at room temperature varied from a minimum of 1.67 kG to a maximum of 2 kG. Past studies reported $4\pi M_s$ as high as 2.56 kG in YIG films [30,51] and were attributed to distribution and/or ionic states of Fe.

The FMR data on the effective magnetization $4\pi M_{eff}$ and the saturation magnetization values in Table 2 can be used to estimate the growth-induced anisotropy field H_u. The effective magnetization $4\pi M_{eff} = 4\pi M_s + (H_c + H_a.)$, where H_c is the magnetocrystalline anisotropy field. As mentioned earlier, H_c is rather small in YIG and is shown to vary from 42 Oe for 9.8 nm YIG film on (100) YAG to 25.6 Oe for 72.7 nm thick film [34] and H_c can be ignored in comparison to the magnitude of H_a. Thus, $H_a = 4\pi M_{eff} - 4\pi M_s$. Values of H_a determined from the FMR and magnetization data are listed in Table 3. The field H_a was negative and was perpendicular to the film plane. Our FMR data on resonance fields for in-plane fields did not show any significant dependence on the direction of H and was indicative of negligible uniaxial in-plane growth induced anisotropy. Values of H_a in Table 3 are shown to range from a maximum of 450 Oe for 55 nm-thick film on (100) YAG to a minimum of zero for the 205 nm-thick film on (110) YAG. Further, Table 3 shows a general decrease when film thickness increased. Values of H_a showed a significant departure from both the magnitudes and thickness dependence of strain anisotropy field H_σ estimated from XRD data. H_a showed the expected decrease when film thickness increased. The

strain anisotropy H_σ showed an increase when film thickness increased. Values of H_a were a factor of 2-to-10 smaller than the H_σ values. It is likely that the cause of very high values of H_σ determined from XRD data that are much higher than H_a could be a significant contribution to the strain from the thermal expansion mismatch between the film and substrate. The cause of the difference in both the values and thickness dependence of H_a and H_σ need further investigation. This may involve studies directed at XRD in films as a function of post-annealing temperatures for the films. One expects the data on M vs. H to confirm the presence of PMA in the films. Data on the dependence of $4\pi M$ on H in Figure 5 and in the supplement showed saturation of M for H_s ~ 100–200 Oe for in-plane H and H_s~1.5–2.0 kOe for out-of-plane H. For in-plane H, one expects $H_s > H_a$ and for the out-of-plane field, $H_s > (4\pi M_s - H_a)$. Thus, relatively small H_s for in-plane H and H_s on the order of $4\pi M_s$ for out-of-plane H are indicative of values of H_a close to that of FMR values and much smaller than H_s.

Next, we compared H_a values for our films with past reports for YIG and spinel ferrite films. FMR measurements on films of YIG on (100) YAG with thicknesses of 9.8 nm to 72.7 nm were reported to have H_a that decreased from 1252 Oe to 49 Oe [34]. A recent study on recrystallized PLD films of YIG on (100) YAG reported that H_a decreased from 72 Oe for a 9.6 nm film to 30 on a 56 nm-thick film [32]. Thus, our 55 nm to 380 nm-thick YIG films showed modestly high H_a values compared to previous reports. Films of spinel ferrites such as nickel ferrite (NFO) showed a much higher H_a than YIG films due to an order of magnitude higher magnetostriction. NFO films that were 445 nm thick and deposited by PLD on magnesium gallate substrate had H_a = 11.9 kOe [26]. Zinc- and Al-substituted NFO were 15–53 nm thick on the $MgAl_2O_4$ substrate and showed H_a ~ 10 kOe [27]. Although the YIG films in this study showed H_a to be much smaller than that of spinel ferrite films, our YIG films on (111) YAG showed one of the highest perpendicular anisotropy filed for YIG. Thus, these findings are potentially of interest for applications in sensors and high-frequency devices.

5. Conclusions

This work focuses on the deposition of thin films of YIG on (100), (110), and (111) YAG substrates using PLD techniques and characterization via structural and magnetic measurement techniques. Films with thicknesses between 58–460 nm were annealed at high temperatures. As the film thickness increased, XRD data revealed a decrease in the in-plane lattice constant and an increase in the out-of-plane lattice constant. A growth induced in-plane compressive strain and an out-of-plane tensile strain were inferred from the XRD data. A stripe domain structure for the films was evident from the MFM phase images. Room temperature saturation magnetization values were found to be in general agreement with magnetization for bulk single crystal values. The strain anisotropy field H_σ determined from the XRD data was uniaxial and perpendicular to the film plane and its magnitude increased when film thickness increased. Films on (100) YAG showed the highest values for H_σ. Ferromagnetic resonance studies at 5 to 21 GHz were performed to determine the growth induced anisotropy field H_a for the films. A decrease in H_a with increasing film thickness was evident for the films on all three orientations of the YAG substrates. Estimated values of H_a ranged from a maximum of 450 Oe for the 55 nm films to a minimum of 30 Oe for 380 nm-thick films.

Supplementary Materials: The following supporting information can be downloaded at: https://www.mdpi.com/article/10.3390/jcs6070203/s1.

Author Contributions: Data acquisition: Y.L., P.Z., R.B. and G.S.; analysis: Y.L., P.Z., J.Z., W.Z., M.R.P. and G.S., funding acquisition: P.Z., W.Z., M.R.P., T.Z. and G.S.; project administration: T.Z. and G.S.; manuscript draft preparation: Y.L., P.Z. and G.S. All authors have read and agreed to the published version of the manuscript.

Funding: The research at Oakland University was supported by grants from the National Science Foundation (DMR-1808892, ECCS-1923732) and the Air Force Office of Scientific Research (AFOSR)

Award No. FA9550-20-1-0114. The research at AFRL was partially supported by the Air Force Office of Scientific Research (AFOSR) Award No. FA9550-20RXCOR074, and a Summer Faculty Fellowship for G.S. The research at Hubei University was supported by the China Postdoctoral Science foundation (No. 2020M672315), and the Program of Hubei Key Laboratory of Ferro- & Piezoelectric Materials and Devices (No. K202013). The research at the Zhengzhou University of Light Industry was supported by the National Science Foundation of China (NSFC, Grant No.61973279).

Institutional Review Board Statement: No approval required.

Informed Consent Statement: Not applicable.

Data Availability Statement: All data generated or analyzed during this study are included in this published article [and its Supplementary Information Files].

Conflicts of Interest: The authors declare no conflict of interest.

References

1. Aichele, T.; Lorenz, A.; Hergt, R.; Görnert, P. Garnet layers prepared by liquid phase epitaxy for microwave and magneto-optical applications—A review. *Cryst. Res. Technol. J. Exp. Ind. Crystallogr.* **2003**, *38*, 575–587. [CrossRef]
2. Gilleo, M.A.; Geller, S. Magnetic and Crystallographic Properties of Substituted Yttrium-Iron Garnet, 3 Y_2O_3 xM_2O_3·(5 − x) Fe_2O_3. *Phys. Rev.* **1958**, *110*, 73. [CrossRef]
3. Gorbatov, O.I.; Johansson, G.; Jakobsson, A.; Mankovsky, S.; Ebert, H.; di Marco, I.; Minár, J.; Etz, C. Magnetic exchange interactions in yttrium iron garnet: A fully relativistic first-principles investigation. *Phys. Rev. B* **2021**, *104*, 174401. [CrossRef]
4. Yudeuk, K.; Bang, D.J.; Kim, Y.; Kim, K.H. Magneto-optical properties of spin-coated bismuth-substituted yttrium iron garnet films on silicon substrates at 1550-nm wavelength. *AIP Adv.* **2020**, *10*, 025306.
5. Kuila, M.; Deshpande, U.; Choudhary, R.J.; Rajput, P.; Phase, D.M.; Raghavendra Reddy, V. Raghavendra Reddy. Study of magneto-optical activity in cerium substituted yttrium iron garnet (Ce: YIG) epitaxial thin films. *J. Appl. Phys.* **2021**, *129*, 093903. [CrossRef]
6. Hansen, P.; Witter, K.; Tolksdorf, W. Magnetic and magneto-optic properties of lead-and bismuth-substituted yttrium iron garnet films. *Phys. Rev. B* **1983**, *27*, 6608. [CrossRef]
7. Serga, A.A.; Chumak, A.V.; Hillebrands, B. YIG magnonics. *J. Phys. D Appl. Phys.* **2010**, *43*, 264002. [CrossRef]
8. Krupka, J.; Salski, B.; Kopyt, P.; Gwarek, W. Electrodynamic study of YIG filters and resonators. *Sci. Rep.* **2016**, *6*, 34739. [CrossRef]
9. Costa, J.D.; Figeys, B.; Sun, X.; Van Hoovels, N.; Tilmans, H.A.; Ciubotaru, F.; Adelmann, C. Compact tunable YIG-based RF resonators. *Appl. Phys. Lett.* **2021**, *118*, 162406. [CrossRef]
10. Tu, C.; Chu, Z.Q.; Spetzler, B.; Hayes, P.; Dong, C.Z.; Liang, X.F.; Chen, H.-H.; He, Y.-F.; Wei, Y.-Y.; Lisenkov, I.; et al. Mechanical-resonance-enhanced thin-film magnetoelectric heterostructures for magnetometers, mechanical antennas, tunable RF inductors, and filters. *Materials* **2019**, *12*, 2259. [CrossRef]
11. Souza, A.L.; Gamino, M.; Ferreira, A.; de Oliveira, A.B.; Vaz, F.; Bohn, F.; Correa, M.A. Directional field-dependence of magnetoimpedance effect on integrated YIG/Pt-stripline system. *Sensors* **2021**, *21*, 6145. [CrossRef] [PubMed]
12. Srinivasan, G.; de Vreugd, C.P.; Bichurin, M.I.; Petrov, V.M. Magnetoelectric interactions in bilayers of yttrium iron garnet and lead magnesium niobate-lead titanate: Evidence for strong coupling in single crystals and epitaxial films. *Appl. Phys. Lett.* **2005**, *86*, 222506. [CrossRef]
13. Yang, X.; Gao, Y.; Wu, J.; Zhou, Z.; Beguhn, S.; Nan, T.; Sun, N.X. Voltage tunable multiferroic phase shifter with YIG/PMN-PT heterostructure. *IEEE Microw. Wirel. Compon. Lett.* **2014**, *24*, 191–193. [CrossRef]
14. Murthy, D.V.B.; Srinivasan, G. Broadband ferromagnetic resonance studies on influence of interface bonding on magnetoeletric effects in ferrite-ferroelectric composites. *Front. Phys.* **2012**, *7*, 418–423.
15. Lisnevskaya, I.V.; Aleksandrova, I.A. Magnetoelectric composites of lead-free piezoelectrics and yttrium iron garnet: Interfacial reactions and functional properties. *Appl. Phys. A* **2020**, *126*, 406. [CrossRef]
16. Litvinenko, A.; Sethi, P.; Murapaka, C.; Jenkins, A.; Cros, V.; Bortolotti, P.; Ferreira, R.; Dieny, B.; Ebels, U. Analog and Digital Phase Modulation and Signal Transmission with Spin-Torque Nano-Oscillators. *Phys. Rev. Appl.* **2021**, *16*, 024048. [CrossRef]
17. Zhang, H.; Ku, M.J.H.; Casola, F.; Du, C.H.R.; van der Sar, T.; Onbasli, M.C.; Ross, C.A.; Tserkovnyak, Y.; Yacoby, A.; Walsworth, R.L. Spin-torque oscillation in a magnetic insulator probed by a single-spin sensor. *Phys. Rev. B* **2020**, *102*, 024404. [CrossRef]
18. Harris, V.G.; Sokolov, A.S. The self-biased circulator: Ferrite materials design and process considerations. *J. Supercond. Nov. Magn.* **2019**, *32*, 97–108. [CrossRef]
19. Ohnuma, M.; Hono, K.; Yanai, T.; Fukunaga, H.; Yoshizawa, Y. Direct evidence for structural origin of stress-induced magnetic anisotropy in Fe–Si–B–Nb–Cu nanocrystalline alloys. *Appl. Phys. Lett.* **2003**, *83*, 2859–2861. [CrossRef]
20. Kurlyandskaya, G.V.; Lukshina, V.A.; Larranaga, A.; Orue, I.; Zaharova, A.A.; Shishkin, D.A. Induced magnetic anisotropy features in FeCrSiBNbCu nanocrystalline alloy: Role of stress distribution proven by direct X-ray measurements. *J. Alloys Compd.* **2013**, *566*, 31–36. [CrossRef]
21. Kubota, M.; Shibuya, K.; Tokunaga, Y.; Kagawa, F.; Tsukazaki, A.; Tokura, Y.; Kawasaki, M. Systematic control of stress-induced anisotropy in pseudomorphic iron garnet thin films. *J. Magn. Magn. Mater.* **2013**, *339*, 63–70. [CrossRef]

22. Quindeau, A.; Avci, C.O.; Liu, W.; Sun, C.; Mann, M.; Tang, A.S.; Onbasli, M.C.; Bono, D.; Voyles, P.M.; Xu, Y.; et al. $Tm_3Fe_5O_{12}$/Pt heterostructures with perpendicular magnetic anisotropy for spintronic applications. *Adv. Electron. Mater.* **2017**, *3*, 1600376. [CrossRef]
23. Soumah, L.; Beaulieu, N.; Qassym, L.; Carrétéro, C.; Jacquet, E.; Lebourgeois, R.; Youssef, J.B.; Bortolotti, P.; Cros, V.; Anane, A. Ultra-low damping insulating magnetic thin films get perpendicular. *Nat. Commun.* **2018**, *9*, 3355. [CrossRef] [PubMed]
24. Bhoi, B.; Kim, B.; Kim, Y.; Kim, M.-K.; Lee, J.-H.; Kim, S. Stress-induced magnetic properties of PLD-grown high-quality ultrathin YIG films. *J. Appl. Phys.* **2018**, *123*, 203902. [CrossRef]
25. Popova, E.; Keller, N.; Gendron, F.; Thomas, L.; Brianso, M.-C.; Guyot, M.; Tessier, M.; Parkin, S.S.P. Perpendicular magnetic anisotropy in ultrathin yttrium iron garnet films prepared by pulsed laser deposition technique. *J. Vac. Sci. Technol. A Vac. Surf. Film.* **2001**, *19*, 2567–2570. [CrossRef]
26. Singh, A.V.; Khodadadi, B.; Mohammadi, J.B.; Keshavarz, S.; Mewes, T.; Negi, D.S.; Datta, R.; Galazka, Z.; Uecker, R.; Gupta, A. Bulk Single Crystal-Like Structural and Magnetic Characteristics of Epitaxial Spinel Ferrite Thin Films with Elimination of Antiphase Boundaries. *Adv. Mater.* **2017**, *29*, 1701222. [CrossRef]
27. Emori, S.; Gray, B.A.; Jeon, H.-M.; Peoples, J.; Schmitt, M.; Mahalingam, K.; Hill, M.; McConney, M.E.; Gray, M.T.; Alaan, U.S.; et al. Coexistence of low damping and strong magnetoelastic coupling in epitaxial spinel ferrite thin films. *Adv. Mater.* **2017**, *29*, 1701130. [CrossRef]
28. Mee, J.E.; Archer, J.L.; Meade, R.H.; Hamilton, T.N. Chemical vapor deposition of epitaxial YIG on YAG and epitaxial GdIG on YAG. *Appl. Phys. Lett.* **1967**, *10*, 289–291. [CrossRef]
29. Zeyfang, R. Stresses in Epitaxially Grown Single-Crystal Films: YIG on YAG. *J. Appl. Phys.* **1970**, *41*, 3718–3721. [CrossRef]
30. Aida, H.; Watanuki, R.; Ito, A. High-speed epitaxial growth of $Y_3Fe_5O_{12}$ thick film with high magnetization on (4 2 0) $Y_3Al_5O_{12}$ substrate using metal-organic chemical vapor deposition. *Mater. Lett.* **2020**, *276*, 128228. [CrossRef]
31. Cooper, J.F.K.; Kinane, C.J.; Langridge, S.; Ali, M.; Hickey, B.J.; Niizeki, T.; Uchida, K.; Saitoh, E.; Ambaye, H.; Glavic, A. Unexpected structural and magnetic depth dependence of YIG thin films. *Phys. Rev. B* **2017**, *96*, 104404. [CrossRef]
32. Krysztofik, A.; Özoğlu, S.; McMichael, R.D.; Coy, E. Effect of strain-induced anisotropy on magnetization dynamics in $Y_3Fe_5O_{12}$ films recrystallized on a lattice-mismatched substrate. *Sci. Rep.* **2021**, *11*, 14011. [CrossRef] [PubMed]
33. Sposito, A.; May-Smith, T.C.; Stenning, G.B.G.; de Groot, P.A.J.; Eason, R.W. Pulsed laser deposition of high-quality μm-thick YIG films on YAG. *Opt. Mater. Express* **2013**, *3*, 624–632. [CrossRef]
34. Wang, H.; Du, C.; Hammel, P.C.; Yang, F. Strain-tunable magnetocrystalline anisotropy in epitaxial $Y_3Fe_5O_{12}$ thin films. *Phys. Rev. B* **2014**, *89*, 134404. [CrossRef]
35. Zanjani, S.M.; Onbaşlı, M.C. Predicting new iron garnet thin films with perpendicular magnetic anisotropy. *J. Magn. Magn. Mater.* **2020**, *499*, 166108. [CrossRef]
36. Van, P.C.; Surabhi, S.; Dongquoc, V.; Kuchi, R.; Yoon, S.G.; Jeong, J.R. Effect of annealing temperature on surface morphology and ultralow ferromagnetic resonance linewidth of yttrium iron garnet thin film grown by rf sputtering. *Appl. Surf. Sci.* **2018**, *435*, 377–383. [CrossRef]
37. Venkatesan, T.; Harshavardhan, K.S.; Strikovski, M.; Kim, J. Recent advances in the deposition of multi-component oxide films by pulsed energy deposition. In *Thin Films and Heterostructures for Oxide Electronics*; Springer: Boston, MA, USA, 2005; pp. 385–413.
38. Popova, E.; Keller, N.; Jomard, F.; Thomas, L.; Brianso, M.-C.; Gendron, F.; Guyot, M.; Tessier, M. Exchange coupling in ultrathin epitaxial yttrium iron garnet films. *Eur. Phys. J. B-Condens. Matter Complex Syst.* **2003**, *31*, 69–74. [CrossRef]
39. Henry, R.; Besser, P.; Heinz, D.; Mee, J. Ferromagnetic resonance properties of LPE YIG films. *IEEE Trans. Magn.* **1973**, *9*, 535–537. [CrossRef]
40. Boudiar, T.; Payet-Gervy, B.; Blanc-Mignon, M.F.; Rousseau, J.J.; Le Berre, M.; Joisten, H. Magneto-optical properties of yttrium iron garnet (YIG) thin films elaborated by radio frequency sputtering. *J. Magn. Magn. Mater.* **2004**, *284*, 77–85. [CrossRef]
41. Wynne, R.; Daneu, J.L.; Fan, T.Y. Thermal coefficients of the expansion and refractive index in YAG. *Appl. Opt.* **1999**, *38*, 3282–3284. [CrossRef]
42. Krichevtsov, B.B.; Gastev, S.V.; Suturin, S.M.; Fedorov, V.V.; Korovin, A.M.; Bursian, V.E.; Banshchikov, A.G.; Volkov, M.P.; Tabuchi, M.; Sokolov, N.S. Magnetization reversal in YIG/GGG (111) nanoheterostructures grown by laser molecular beam epitaxy. *Sci. Technol. Adv. Mater.* **2017**, *18*, 351–363. [CrossRef] [PubMed]
43. Lutsev, L.V.; Korovin, A.M.; Suturin, S.M.; Vlasenko, L.S.; Volkov, M.P.; Sokolov, N.S. Spin excitations in laser-molecular-beam epitaxy-grown nanosized YIG films: Towards low relaxation and desirable magnetization profile. *J. Phys. D Appl. Phys.* **2020**, *53*, 265003. [CrossRef]
44. Krichevtsov, B.B.; Korovin, A.M.; Gastev, S.V.; Suturin, S.M.; Mashkov, K.V.; Sawada, M.; Sokolov, N.S. Magnetization reversal in Co/GGG/YIG/GGG (111) nanoheterostructures: Interlayer magnetic coupling and orange peel effect. *J. Magn. Magn. Mater.* **2020**, *502*, 166542. [CrossRef]
45. Krichevtsov, B.B.; Bursian, V.E.; Gastev, S.V.; Korovin, A.M.; Lutsev, L.V.; Suturin, S.M.; Mashkov, K.V.; Volkov, M.P.; Sokolov, N.S. Substrate induced magnetic anisotropies and magneto-optical response in YIG nanosized epitaxial films on NdGG (111). *arXiv* **2018**, arXiv:1901.10800.
46. Komogortsev, S.V.; Vazhenina, I.G.; Kleshnina, S.A.; Iskhakov, R.S.; Lepalovskij, V.N.; Pasynkova, A.A.; Svalov, A.V. Advanced Characterization of FeNi-Based Films for the Development of Magnetic Field Sensors with Tailored Functional Parameters. *Sensors* **2022**, *22*, 3324. [CrossRef]

47. Von Aulock, W.H. *Handbook of Microwave Ferrite Materials*; Academic Press: London, UK, 1965.
48. Barandiarán, J.M.; García-Arribas, A.; de Cos, D. Transition from quasistatic to ferromagnetic resonance regime in giant magnetoimpedance. *J. Appl. Phys.* **2006**, *99*, 103904. [CrossRef]
49. Shcherbinin, S.V.; Svalov, A.V.; Melnikov, G.Y.; Kurlyandskaya, G.V. Angular dependence of the ferromagnetic resonance parameters of $[Ti/FeNi]_6/Ti/Cu/Ti/[FeNi/Ti]_6$ nanostructured multilayered elements in the wide frequency range. *Nanomaterials* **2020**, *10*, 433. [CrossRef]
50. Beguhn, S.; Zhou, Z.; Rand, S.; Yang, X.; Lou, J.; Sun, N.X. A new highly sensitive broadband ferromagnetic resonance measurement system with lock-in detection. *J. Appl. Phys.* **2012**, *111*, 07A503. [CrossRef]
51. Gallagher, J.C.; Yang, A.S.; Brangham, J.T.; Esser, B.D.; White, S.P.; Page, M.R.; Meng, K.-Y.; Yu, S.; Adur, R.; Ruane, W.; et al. Exceptionally high magnetization of stoichiometric $Y_3Fe_5O_{12}$ epitaxial films grown on $Gd_3Ga_5O_{12}$. *Appl. Phys. Lett.* **2016**, *109*, 072401. [CrossRef]